



Effect of thermal treatment on TiO₂ nanorod electrodes prepared by the solvothermal method for dye-sensitized solar cells: Surface reconfiguration and improved electron transport



Jingyong Zhao^{a,b}, Jianxi Yao^{a,b,*}, Yongzhe Zhang^{a,b,*}, Mina Guli^{a,b}, Li Xiao^{a,b}

^a State Key Laboratory of Alternate Electrical Power System with Renewable Energy Sources, North China Electric Power University, Beijing 102206, China

^b The New and Renewable Energy of Beijing Key Laboratory, Renewable Energy School, North China Electric Power University, Beijing 102206, China

HIGHLIGHTS

- TiO₂ nanorods arrays were prepared by the solvothermal method and applied to DSSCs.
- The effect of thermal treatment on the solvothermal method has been studied in detail.
- Thermal treatment could significantly change the morphology and surface condition of TNRs.
- Thermal treatment leads to 39% improvement of η for the nanorods based DSSCs.

ARTICLE INFO

Article history:

Received 6 November 2013

Received in revised form

25 December 2013

Accepted 30 December 2013

Available online 8 January 2014

Keywords:

Solvothermal method

Thermal treatment

Surface reconfiguration

Titanium dioxide nanorod arrays

Dye-sensitized solar cells

ABSTRACT

Solvothermal synthesis is considered a novel method of preparing the photoanode in dye-sensitized solar cells (DSSCs), which can directly synthesize material with good crystallinity at low temperatures without thermal treatment. However, how thermal treatment influences the properties of the materials synthesized by this method is still unclear, especial at the microscopic level. In this study, we applied TiO₂ nanorod arrays prepared by the solvothermal method to DSSCs. X-ray Diffraction (XRD) and Raman results indicate that the crystal structure of TiO₂ nanorods did not change after thermal treatment. However, the photovoltaic performance improved by 39%. Detailed analysis of high-resolution transmission electron microscopy (HRTEM) results demonstrate that a surface reconfiguration occurred, shifting one thin amorphous TiO₂ layer to tiny crystallite spheres. The X-ray photoelectron spectroscopy (XPS) and Fourier transform infrared spectroscopy (FTIR) measurements further confirm this morphology change, and the surface states also become more suitable for dye absorption, which leads to a significant improvement in efficiency. Moreover, good electrical transport is observed due to the low concentration of surface defects. Therefore, we believe the performance improvement comes from crystalline surface and surface chemical bonding improvements. Our results could be useful in photo-electrical applications of the solvothermal synthesis method.

Crown Copyright © 2014 Published by Elsevier B.V. All rights reserved.

1. Introduction

Dye-sensitized solar cells (DSSCs) have attracted extensive interest in the last two decades, due to their advantages of low cost, no pollution and relatively high energy conversion efficiency [1–5]. The photoanode is a key component of DSSCs, it acts as a scaffold for the dyes and a transfer media for photogenerated electrons to

* Corresponding authors. State Key Laboratory of Alternate Electrical Power System with Renewable Energy Sources, North China Electric Power University, Beijing 102206, China.

E-mail addresses: jianxiyao_ncepu@126.com (J. Yao), yyzhang@ncepu.edu.cn (Y. Zhang).

the F-doped tin oxide (FTO) layer. Generally, a TiO₂ nanoparticle film is used for the photoanode in high-efficiency DSSCs due to the large specific surface areas. However, electron scattering and trapping in the grain boundaries among nanoparticles seriously influence DSSCs performance [6]. Vertically aligned one-dimensional nanostructures such as nanowire/nanorod/nanotube arrays prepared by the solvothermal method have shown great advantages. It has been proven that one-dimensional nanostructures have a diffusion rate that is several orders of magnitude higher than that of nanoparticles [7,8]. The solvothermal method seems to be a promising approach that does not require additional thermal treatment to prepare single-crystal one-dimensional nanostructures. Moreover, many reports have claimed that

photoanodes with good crystallinity can be directly prepared on a flexible substrate irrespective of the annealing process using this approach [9].

However, thermal treatment is generally considered an effective strategy to improve the material's crystallinity. Moreover, the surface conditions, such as functional groups and surface states, are also modified during the thermal process. Zhu et al. found that thermal treatment makes the nanotube arrays prepared by the anodic oxidation method transform from an amorphous phase to a fully crystalline phase. The crystallinity improved the electron transport and decreased electron recombination [10]. Yang et al. found that some functional groups related to carbon, nitrogen and hydrogen were released from the surfaces of nanorod arrays after thermal treatment. The surface and deep-level nanorod defects were also decreased [11]. Zhao et al. found that thermal treatment could increase the carrier mobility and conductivity of ZnO nanorods by reducing the surface oxygen defects [12]. In DSSCs, good crystallinity and surface conditions could increase the photoelectron transport rate and the amount of dye absorption, thereby improving the energy conversion efficiency. However, how does the thermal treatment influence the nanostructures prepared by solvothermal method, which is much important, has not yet been elucidated especially in microscale level.

In this study, TiO₂ nanorod arrays (TNRs) were synthesized directly on FTO glass through the solvothermal method, and thermal treatments were subsequently performed. The effect of thermal treatment on the crystal structure, morphology and surface condition of TNRs was investigated in detail. The results show that the crystal structure does not change due to thermal treatment. However, the surface morphology appears to change significantly from a thin amorphous layer to tiny crystallite spheres. Moreover, surface defects and chemical bonding are removed. All of these changes lead to a 39% improvement in the photoelectric conversion efficiency for the nanorod-based DSSCs. These findings might be useful in photoelectrical applications of the solvothermal method.

2. Experimental

2.1. Preparation of TiO₂ nanorod arrays

First, well-cleaned FTO substrate was immersed into an aqueous solution of 0.05 M TiCl₄ at 70 °C for 30 min to form a compact layer. The film was annealed in air at 500 °C for 30 min. To grow TiO₂ nanorods, tetrabutyl titanate (Ti(OC₄H₉)₄, CP Sinopharm Chemical Reagent Beijing Co., Ltd), hydrochloric acid (HCl, 37% by weight, Beijing Chemical Works) and n-hexane (CH₃(CH₂)₄CH₃, AR, Sinopharm Chemical Reagent Beijing Co., Ltd) were used as the titanium precursor, acidic medium and solvent, respectively. In a typical synthesis process, n-hexane, tetrabutyl titanate and hydrochloric acid at a molar ratio of 77:4:11 were mixed under magnetic stirring. Subsequently, the mixed solution was transferred to a stainless steel autoclave (40 ml volume) with a Teflon liner, and the FTO substrate was placed against the wall of the Teflon liner with the conducting surface facing down. Then, the autoclave was sealed and maintained at 180 °C for 15 h followed by natural cooling to room temperature. The as-grown sample was rinsed with deionized water and absolute ethanol and then dried in ambient air. To study the influence of annealing, the as-grown samples were annealed at 200 °C, 400 °C and 500 °C for 30 min.

2.2. Assembly of DSSCs

The TiO₂ nanorod arrays were immersed in a 5×10^{-4} M ethanol solution of ruthenium 535-bisTBA (N719 dye, Wuhan Geao) at 45 °C for 24 h. Subsequently, the photoanode was rinsed with anhydrous

ethanol to remove the extra dye at room temperature. After that, the dye-sensitized photoanode and a Pt-coated FTO counter electrode (Wuhan Geao) were clamped using a face-to-face layout. A drop of the electrolyte, a solution containing of 0.5 M LiI, 0.05 M I₂, 0.5 M 4-tert-butyl pyridine (TBP) and 0.3 M dimethyl phthalate (DMPII) in 10 ml acetonitrile, was injected into the space between the two electrodes. The active area of the solar cells was 0.25 cm².

2.3. Characterization

The morphology of TiO₂ nanorod films was characterized by scanning electron microscopy (SEM, FEI Quanta200F, Operating voltage: 30 kV). The crystal structure of the nanorods was examined using Raman spectroscopy (RFS100, BRUKER) and X-ray Diffractometer (XRD, D8 ADVANCE, Cu K α radiation, $\lambda = 1.54$ Å, tube voltage = 40 kV, tube current = 30 mA). The photocurrent density–voltage characteristics of the DSSCs were evaluated by a source meter (Keithley 2400) under a solar simulator (Oriel 92250A-1000, Newport, 100 mW cm⁻²). The amounts of absorbed dye were measured using a UV–visible Spectrophotometer (UV-2450, Shimadzu) by desorbing the dye from TiO₂ nanorod films in a 0.1 M NaOH water solution. High-resolution transmission electron microscopy (HRTEM) and selected-area electron diffraction (SAED) analyses were performed on a high-resolution transmission electron microscope (JEOL JEM-2000FX, Japan). The surface properties of prepared samples were characterized by X-ray photoelectron spectroscopy (XPS, Thermo Fisher, K-Alpha). To investigate the chemical bonding on the TNRs surface, Fourier transform infrared spectroscopy (FTIR, Perkin Elmer, Spectrum100) was performed at a resolution of 0.5 cm⁻¹. The electrochemical performance was investigated with a CHI660D instrument at open-circuit potential from 0.01 to 10⁵ Hz under one sun light. The magnitude of the alternative signal was 10 mV. The electrical impedance spectra were analyzed using Z-View software. *I*–*V* measurements were performed using a Keithley 2400 source meter.

3. Result and discussion

The FESEM images of the as-grown TNRs and the TNRs annealed at 200 °C, 400 °C and 500 °C are shown in Fig. 1. As shown in Fig. 1(a1) and (a2), the FTO glass is uniformly covered with TiO₂ nanorods, and the interspaces between nanorods is narrow. The TNRs is highly ordered, well oriented and vertical to the substrate. The thickness of TiO₂ film is approximately 3 μ m. After thermal treatment, the morphologies of nanorods do not show any change in the density, length, and size.

The crystal structure was determined by Raman and XRD as shown in Fig. 2. Four obvious Raman peak are observed at 143 cm⁻¹, 234 cm⁻¹, 446 cm⁻¹ and 609 cm⁻¹ for all samples. The Raman results indicate that all of the samples have a highly crystalline rutile structure. The rutile structure belongs to the P4₂/mnm tetragonal space group with the following five Raman active modes: B_{1g}, E_g, A_{1g}, B_{2g}, and second-order scattering [13]. The peaks at 143 cm⁻¹, 446 cm⁻¹ and 609 cm⁻¹ can be attributed to the Raman active modes B_{1g}, E_g and A_{1g} of rutile TiO₂, respectively. The broad band located at 234 cm⁻¹ comes from second-order scattering [13,14].

Fig. 2(b) shows the XRD patterns of the FTO substrate, as-grown TNRs and the TNRs annealed at 500 °C. For the as-grown TNRs, two peaks corresponding to the (101) and (002) planes of tetragonal rutile TiO₂ (JCPDS no. 21-1276) have been identified at 36.00° and 62.77°, respectively. All the other peaks come from the FTO substrate. The (002) peak is significantly enhanced, indicating that the nanorods are well crystallized and grow preferentially along the [001] direction with a growth axis perpendicular to the substrate [15]. Moreover, some diffraction peaks including (110), (211) and

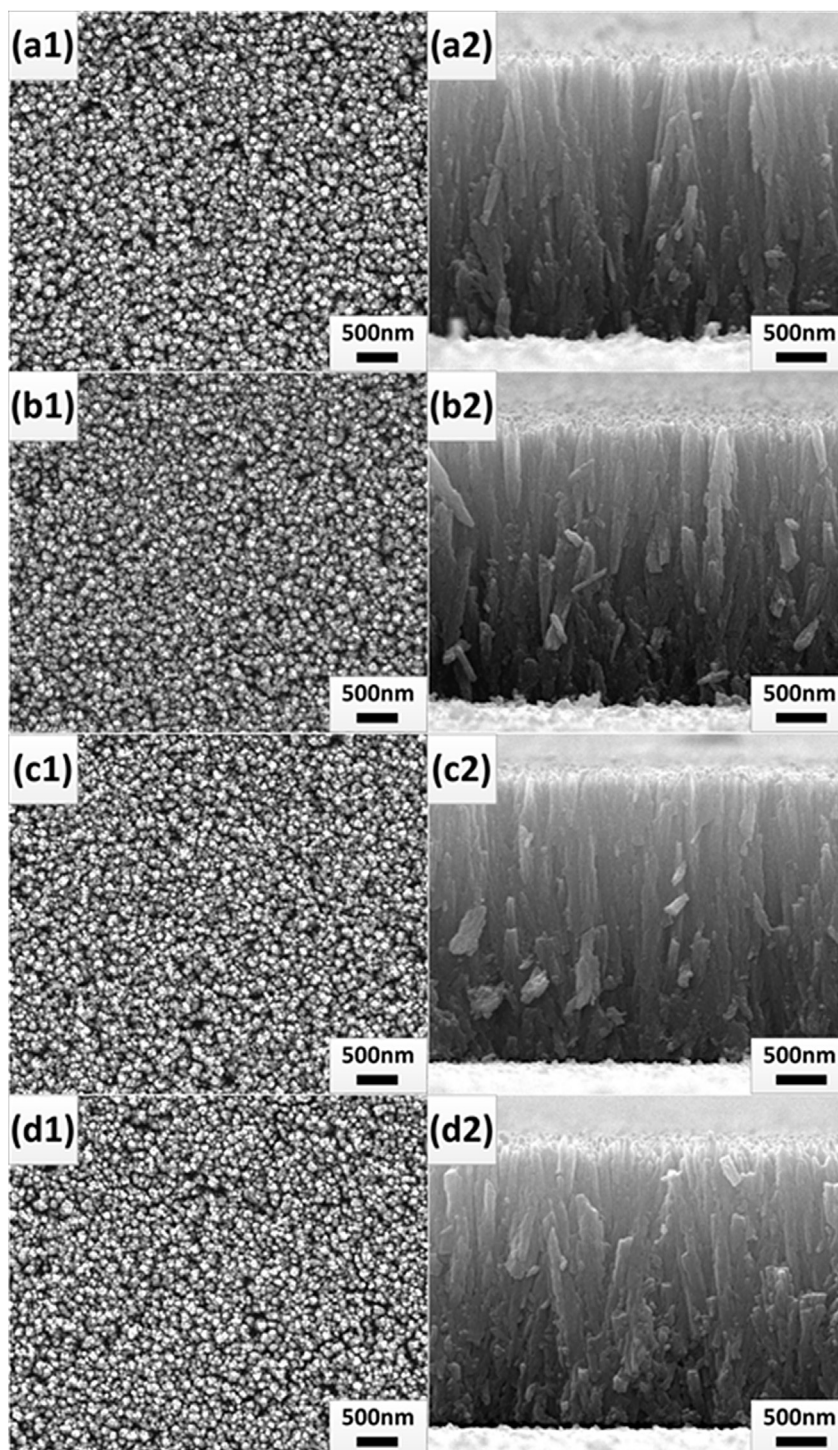


Fig. 1. FESEM images of TNRs. (a1), (b1), (c1) and (d1) are top views of as-grown TNRs and the TNRs annealed at 200 °C, 400 °C, and 500 °C. (a2), (b2), (c2) and (d2) are cross-sectional views.

(111), which are normally present in polycrystalline or powder samples are absent, which reveals that the nanorods are not only vertically aligned but also a single crystalline throughout their length [6,16]. The patterns of TNRs annealed at 500 °C show the same characteristics as as-grown TNRs, which shows that thermal treatment does not influence the TiO_2 crystal structure, in agreement with the Raman results.

To investigate the effect of thermal treatment on the photovoltaic properties of DSSCs, photo-electrodes made from as-grown

TNRs and the TNRs annealed at different temperature were prepared. Fig. 3 shows the photocurrent–voltage (J – V) curves of these cells, and the results are summarized in Table 1. It is interesting that the efficiency increases from 2.31% to 3.21%, a 39% improvement after annealing at 500 °C. Although the crystal structure of the sample does not show any change after thermal treatment, the photovoltaic properties are significantly enhanced. The open circuit voltage (V_{oc}), short-circuit current density (J_{sc}) and fill factor (FF) of the device based on as-grown TNRs were 0.57 V, 7.94 mA cm^{-2} , and

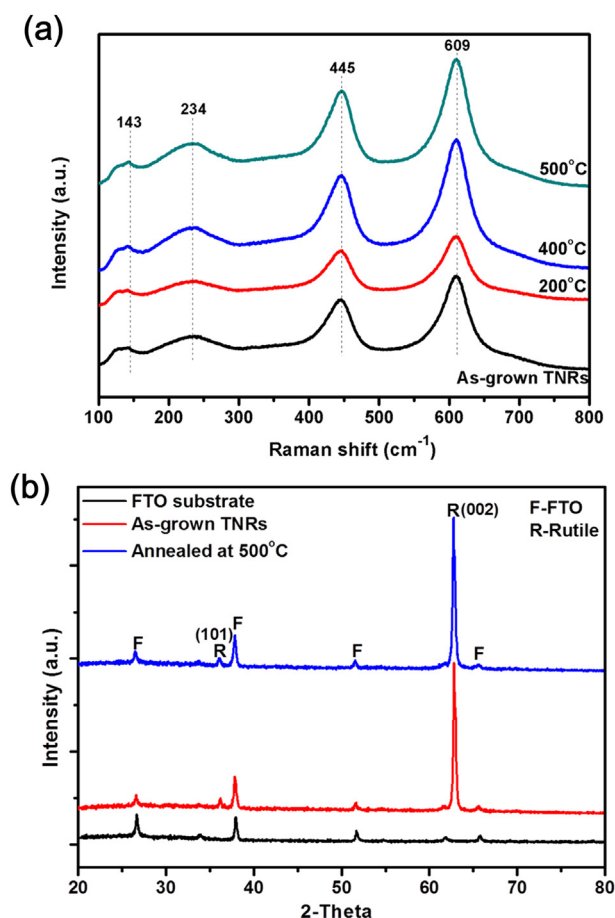


Fig. 2. (a) Raman spectrum of as-grown TNRs and the TNRs annealed at 200 °C, 400 °C and 500 °C; (b) XRD patterns of FTO substrate, as-grown TNRs and TNRs annealed at 500 °C.

0.52, respectively, corresponding to a power conversion efficiency (η) of 2.31%. After annealing at 200 °C, 400 °C and 500 °C, the J_{sc} and η increased with the annealing temperature. When the TNRs are annealed at 500 °C, the highest power conversion efficiency (3.21%) is achieved.

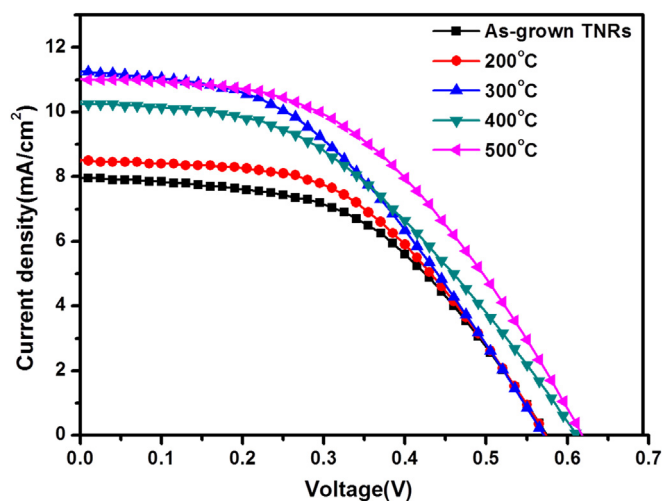


Fig. 3. J – V curves of the DSSCs from as-grown TNRs and TNRs annealed at 200 °C, 400 °C and 500 °C.

Table 1 shows that the improvement is mainly due to the increase in current density, which is usually attributed to more dye absorption and effective electron injection [5,17]. The account of absorbed dye was measured by desorption. The UV–vis absorption spectra of N719 dye in 0.1 M NaOH aqueous solution are shown in Fig. 4. The dye loading in as-grown TNRs and the TNRs annealed at 500 °C were calculated as 5.6×10^{-8} and 6.75×10^{-8} mol cm $^{-2}$ using Lambert–Beer law $A = kbc$, where $k = 1.41 \times 10^4$ L mol $^{-1}$ cm $^{-1}$, k is the molar extinction coefficient of N719 at 500 nm. The amount of dye adsorption increases by 20.5% after thermal treatment. Therefore, the annealed sample has larger J_{sc} and efficiency. Generally, the amount of dye loading depends on the surface area and surface chemical bonding of the photoanode [18]. The dye molecules were chemically adsorbed onto the surface of TiO $_2$ nanorods via the formation of ester-like bonds between the carboxylic acid groups and –OH groups on the TiO $_2$ nanorods [19–21].

The surface conditions of the nanorods were determined by the HRTEM and SAED patterns as shown in Fig. 5(a) and (b). A clear crystal lattice with interplanar spacings $d_{110} = 0.32$ nm and $d_{001} = 0.29$ nm appears, which corresponds to the well-aligned spots shown in the SAED pattern (Fig. 5(b)), indicating that the TiO $_2$ nanorods are single crystal rutile TiO $_2$. After thermal treatment, the same well-aligned spots and lattice fringes are shown in Fig. 5(c) and (d), indicating that the crystal structure of TNRs does not change after thermal treatment, which further confirms the XRD and Raman results. From the HRTEM images and higher magnification shown in Fig. 5(a), it is noted that the surface of as-grown TiO $_2$ nanorods is smooth, and there is an obvious amorphous layer with a thickness of approximately 1 nm covering TiO $_2$ nanorods. Considering the precursor, we believe that the surface coating is amorphous TiO $_2$. After thermal treatment, the amorphous coating layer reconfigured and changed to tiny crystallite nanospheres attached on the surface of TiO $_2$ nanorods. This change has two effects. One is the increase in the specific surface area, which would increase dye adsorption [8,22]; the other is that dye molecules can directly bind to the surface of the crystalline TiO $_2$ nanorods but not the amorphous TiO $_2$ layer, thus improving the photoelectron transfer from the dye to TiO $_2$. As a result, higher J_{sc} and efficiency were achieved from the annealed TNR-based DSSCs.

To obtain detailed information of surface chemical states, XPS measurements were carried out on the as-grown TNRs and the TNRs annealed at 500 °C, as shown in Fig. 6. For the Ti2p XPS spectra (Fig. 6(a) and (b)), the two main peak are located at 458.6 eV and 464.3 eV, which are assigned to Ti $^{4+}$ 2p $_{3/2}$ and Ti $^{4+}$ 2p $_{1/2}$ in TiO $_2$. The shoulder peaks at 457.5 eV and 463.2 eV correspond to Ti $^{3+}$ 2p $_{3/2}$ and Ti $^{3+}$ 2p $_{1/2}$ [23], and their presence was attributed to the surface defect state. The O1s band shows three contributions (Fig. 6(c) and (d)). The main peak was located at 530.0 eV (O1), and it is associated with the lattice oxygen of TiO $_2$. The band at 531.5 eV (O2) is from the oxygen vacancy-Ti $^{3+}$ surface state, also known as Ti $_2$ O $_3$. Finally, the band at 532.5 eV (O3) is commonly attributed to absorbed H $_2$ O or –OH groups on the surface [23–25]. From the fitting of the Ti2p and O1s band, the relative atomic concentration

Table 1

The key J – V characteristics of the DSSCs consist of as-grown TNRs and TNRs annealed at 200 °C, 400 °C and 500 °C.

Cell	Current density (mA cm $^{-2}$)	Voltage (V)	Fill factor	Efficiency (%)
As-grown	7.94	0.57	0.52	2.31
200 °C	8.48	0.57	0.51	2.46
400 °C	10.24	0.61	0.44	2.74
500 °C	11.02	0.61	0.48	3.21

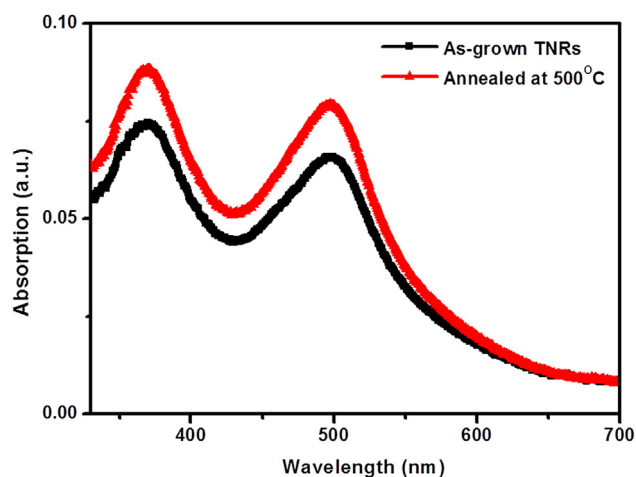


Fig. 4. UV–vis absorption spectra of N719 dye in 0.1 M NaOH aqueous solution, desorbed from the TiO_2 electrodes made with as-grown TNRs and the TNRs annealed at 500 °C.

of each oxygen species and $\text{Ti}2p_{3/2}$ was calculated and listed in Table 2.

After thermal treatment, the percentage of $\text{Ti}^{3+}2p_{3/2}$ ions decreases from 10.9% to 6.3%, and the ratio of $\text{Ti}^{4+}2p_{3/2}$ in TiO_2 increases from 89.1% to 93.7%. These changes are attributed to the disappearance of the amorphous coating on the surface of TNRs and formation of tiny crystallite particles. Meanwhile, due to the amorphous coating, there should be a larger concentration of broken bonds and other defects related to Ti^{3+} , unlike those found in annealed crystalline films [26]. The oxygen vacancy- Ti^{3+} component also decreases from 14.5% to 8.3% after thermal treatment. Generally, the oxygen vacancy- Ti^{3+} defects serve as electron-recombination centers and decrease the open-circuit voltage of DSSCs [27]. Thermal annealing reduces the concentration of surface defects and then decreases the rate of electron recombination. Moreover, the ratio of adsorbed oxygen decreases from 4.1% to 3.2% after thermal treatment. Adsorbed oxygen acts as electron acceptors, trapping free carriers and thus lowering electrical conductivity [28,29]. Therefore, the electrical conductivity of TNRs could be enhanced after thermal treatment.

To investigate the surface chemical bonding of the TNRs, FTIR spectra of as-grown TNRs and the TNRs annealed at 500 °C were

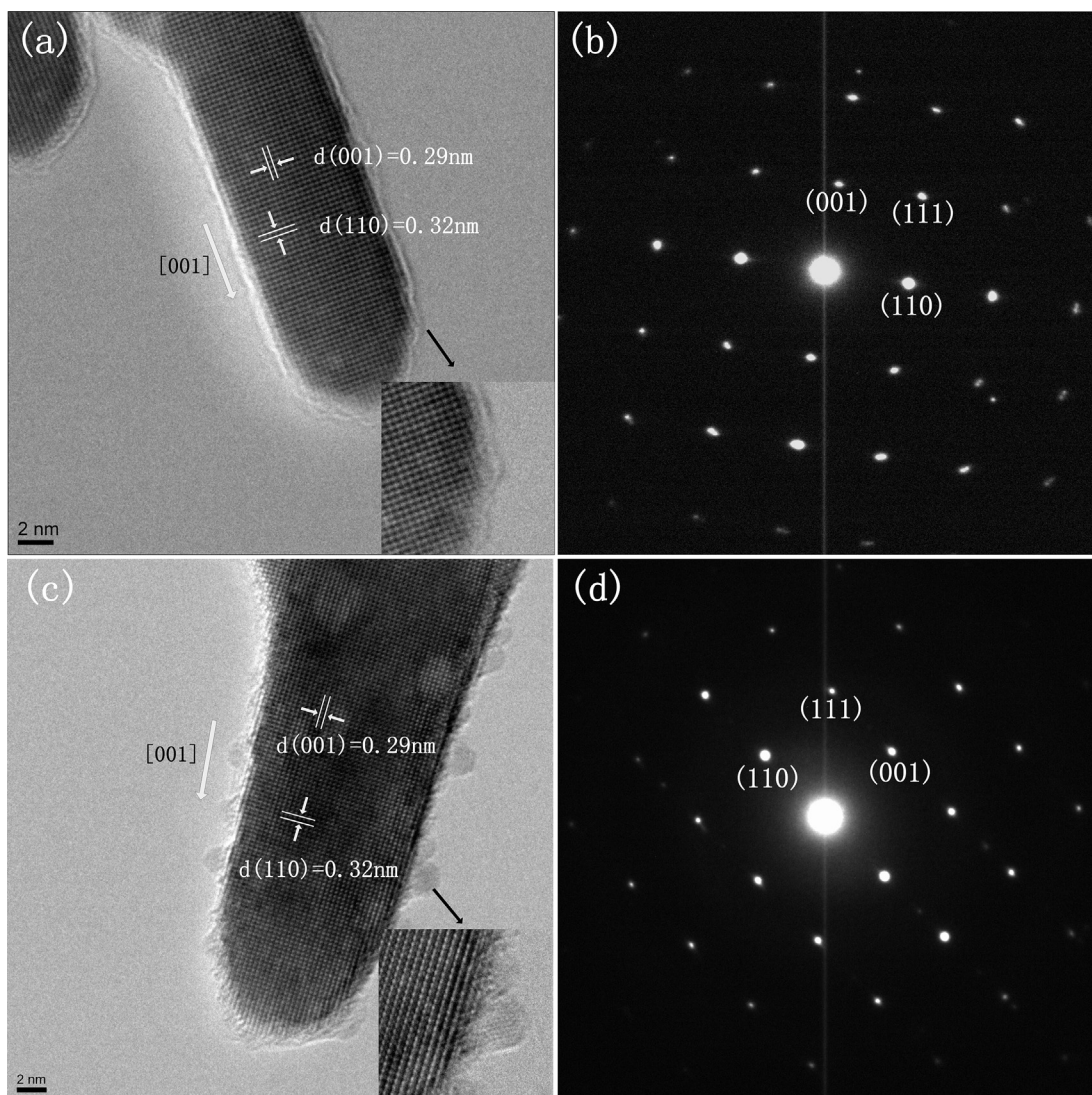


Fig. 5. (a) HRTEM image and (b) SAED image of as-grown TNRs; (c) HRTEM image and (d) SAED image of the TNRs annealed at 500 °C.

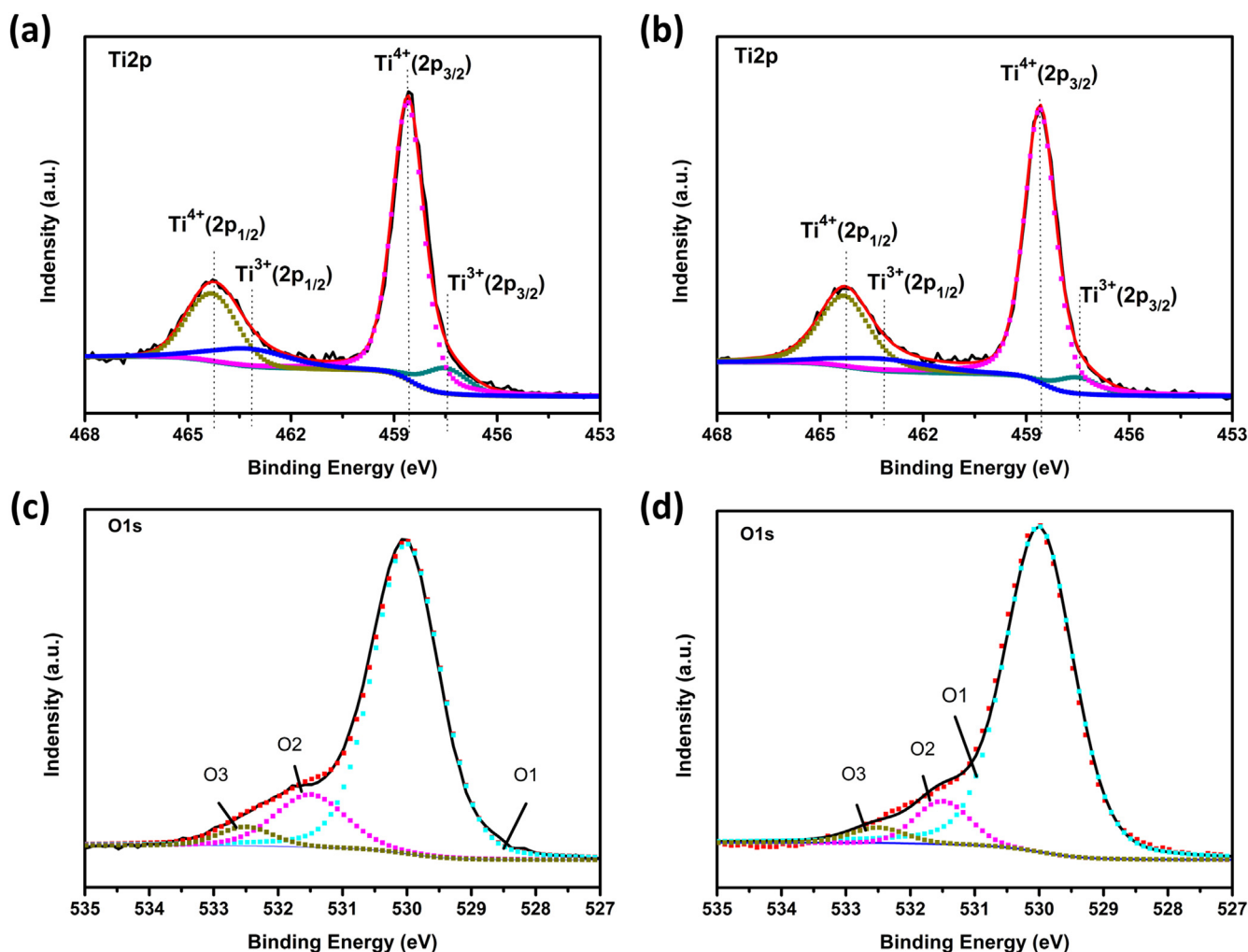


Fig. 6. (a) Ti2p and (c) O1s region of the XPS spectra of as-grown TNRs and (b) Ti2p and (d) O1s region of the XPS spectra of TNRs annealed at 500 °C.

determined and are shown in Fig. 7. For the as-grown sample, six absorption valleys are observed. The bands at 3428 and 1634 cm^{-1} originate from deformation vibrations of water molecule adsorbed on the TiO_2 nanorods surface [30,31]. The band at 1435 cm^{-1} can be attributed to the C–H bending mode, which is due to residual n-hexane [32]. And the band at 1137 cm^{-1} is attributed to Ti–OH deformation vibrations of hydroxyl groups on the TiO_2 surface [33,34]. Another signal located at 627 cm^{-1} is attributed to the Ti–O–Ti bonds in amorphous titanium oxide, and this result is consistent with the HRTEM and XPS findings. The band at 528 cm^{-1} is attributed to the lattice vibrations of TiO_2 [35]. After thermal treatment, the signal related to Ti–O–Ti bonds in amorphous titanium oxide and n-hexane on the surface of the TNRs disappeared. As observed in the HRTEM images, the amorphous surface coating layer changed into tiny crystallite nanospheres after thermal

treatment, so the signals related to this layer disappeared. In addition, amorphous TiO_2 is very hydrophilic [26,36], and it can absorb a great deal of H_2O on the surface of TiO_2 . Therefore, the two peaks corresponding to water molecules from the annealed TNRs sample also disappeared. The hydroxyl groups on the TiO_2 surface did not obviously change. The removal of the adsorbed water and residual n-hexane and the retention of the –OH group are very beneficial for dye absorption.

The electrical transport properties were measured, and the results are shown in Figs. 8 and 9. The dark J – V curves of DSSCs consisting of as-grown TNRs and the TNRs annealed at 500 °C are shown in Fig. 8(a). The DSSCs made of as-grown TNRs show a higher dark current than the TNRs annealed at 500 °C at the same voltage. Thermal treatment can suppresses electron recombination and decrease the dark current, likely due to the decreased of surface state and oxygen vacancy- Ti^{3+} defects of TNRs as shown in the XPS results. To determine the charge transfer properties of DSSCs, electrochemical impedance spectroscopy (EIS) measurements were conducted at an open circuit voltage (V_{oc}) under AM1.5 conditions, and the results are shown in Fig. 8(b). The key EIS characteristics of DSSCs based on as-grown TNRs and TNRs annealed at 500 °C are shown in Table 3. An equivalent circuit, as shown in the inset of Fig. 8(b), is employed to fit all of the hemispheres using Z-view software. R_s is the series resistance accounting for the transport resistance of the TCO glass, contact resistance, and wire resistance

Table 2

XPS binding energies (BE) and chemical composition of as-grown TNRs and the TNRs annealed at 500 °C.

Sample		O1	O2	O3	$\text{Ti}^{4+}2p_{3/2}$	$\text{Ti}^{3+}2p_{3/2}$
As-grown TNRs	BE (eV)	530.0	531.5	532.5	458.6	457.5
	Percentage (%)	81.4	14.5	4.1	89.1	10.9
TNRs annealed at 500 °C	BE (eV)	530.0	531.5	532.5	458.6	457.5
	Percentage (%)	88.5	8.3	3.2	93.7	6.3

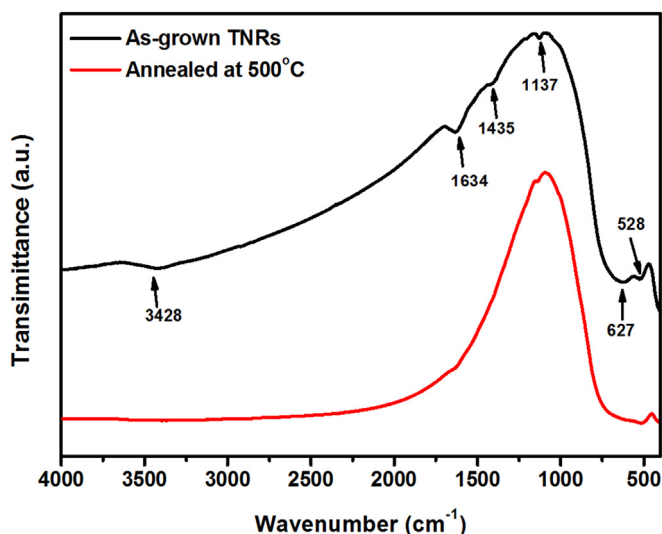


Fig. 7. FTIR spectra of as-grown TNRs and the TNRs annealed at 500 °C.

[37,38]. There is no change in series resistance after thermal treatment. R_1 represents the interfacial resistance of the first hemispheres in the high frequency region of 10^3 – 10^5 Hz, which is related to the charge transfer impedance at the TiO_2 electrode and

Table 3

The key EIS characteristics of the DSSCs based on as-grown TNRs and TNRs annealed at 500 °C.

Sample	Series resistance R_s (Ω)	Interfacial resistance R_1 (Ω)	Interfacial resistance R_2 (Ω)	Electron lifetime τ (s)
As-grown TNRs	20.99	22.55	42.47	0.12
TNRs annealed at 500 °C	21.00	21.85	36.10	0.18

FTO/TiO_2 layer interface. This value is 22.55 Ω and 21.85 Ω in as-grown TNRs and the annealed one, respectively, which is only a slight decrease, indicating that the thermal treatment has small effect on the contact of the FTO and TiO_2 layers. R_2 represents the interfacial resistance of the second hemispheres in the lower frequency region of 1– 10^3 Hz, which is related to the charge transfer impedance at the semiconductor/dye/electrolyte interface [39]. The R_2 of as-grown TNR cells is much larger than that of the DSSCs with annealed TNRs, indicating that the main change occurs in the semiconductor/dye/electrolyte interface, which can be attributed to a significant change in the surface state of the TNRs before and after thermal treatment. Before thermal treatment, there is an amorphous layer that the electrons injected from the dye into TiO_2 need to cross, so the resistance is large. Because the amorphous layer disappeared after thermal treatment, the injection resistance decreased. The electron lifetime (τ) of the TiO_2 film can be determined by the equation $\tau = 1/k_{\text{eff}}$ [40], where k_{eff} is defined as the effective rate constant for recombination, which is estimated from the peak frequency value (ω_{max}) of the middle frequency peak using $k_{\text{eff}} = \omega_{\text{max}}$. ω_{max} was determined as 8.25 Hz and 5.63 Hz for the DSSCs made with as-grown TNRs and annealed ones, so the electron lifetime is 0.12 s and 0.18 s, respectively. The increase in electron lifetime can be attributed to the lower concentration of oxygen vacancy- Ti^{3+} surface defects.

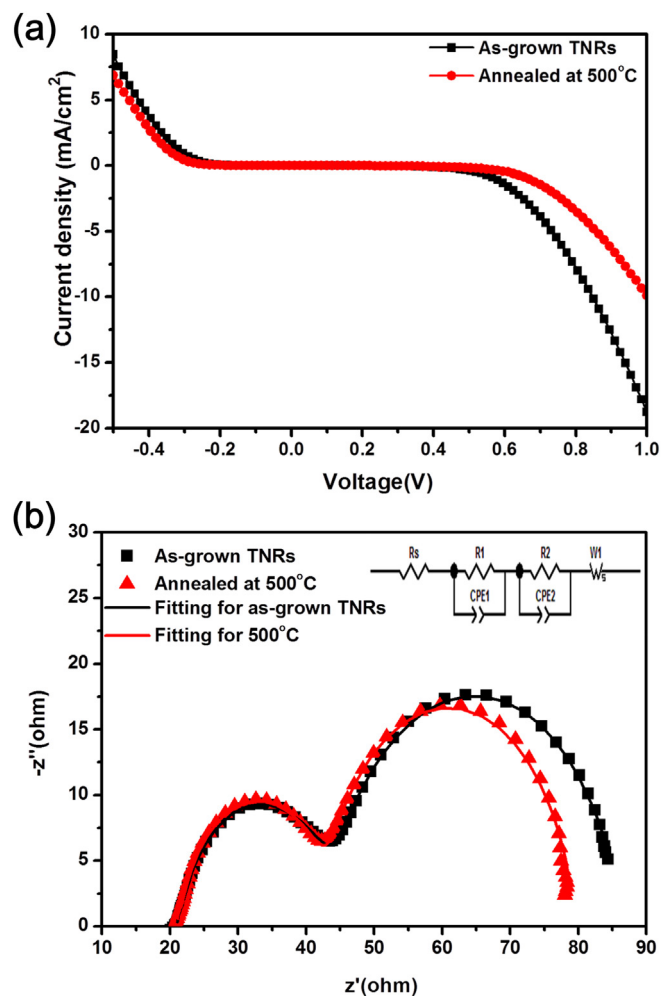


Fig. 8. (a) Dark J – V curves of DSSCs consisting of as-grown TNRs and TNRs annealed at 500 °C; (b) impedance spectra of as-grown TNRs and TNRs annealed at 500 °C.

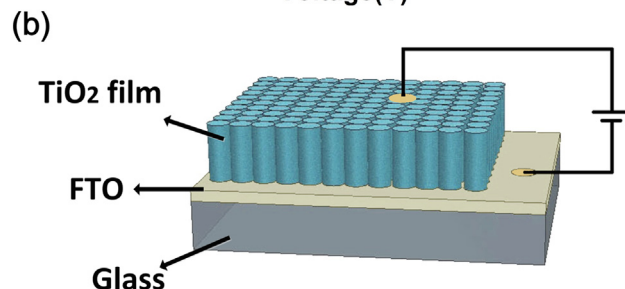
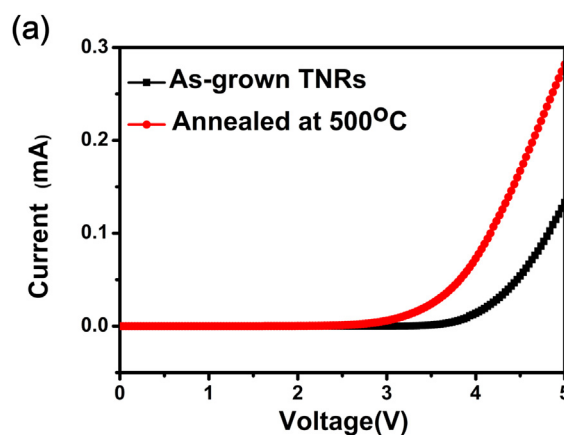


Fig. 9. (a) I – V characteristics of as-grown TNRs and the TNRs annealed at 500 °C; (b) the schematic diagram for I – V measurements.

The current–voltage (I – V) curves of as-grown TNRs and TNRs annealed at 500 °C were used to study their electrical transport properties (Fig. 9). A schematic diagram for I – V measurements is in Fig. 9(b). Two Au electrodes are sputtered on TiO₂ film and FTO, and the area of the Au electrode is 0.02 cm². Then the source meter is connected to the electrode by metal probe. The forward bias voltage was applied to the TiO₂ film. I – V curves showed clear rectifying behavior that can be attributed to the Schottky contact between the electrode and the TNRs [41]. For as-grown TNRs and the annealed ones, the voltage at which current started to flow was in the range 3.15–3.75 V. At positive tip voltages, higher currents were obtained for the annealed TNRs. From the slope of the I – V curves, the electrical resistivity (ρ) for as-grown TNRs and the TNRs annealed at 500 °C was $3.90 \times 10^6 \Omega \text{ cm}$ and $2.89 \times 10^6 \Omega \text{ cm}$, respectively. The values of ρ are given by $\rho = RS/L$, where R is the resistance of the TNRs and is the value of slope, S is the area of the Au electrode, and L is the thickness of TNRs. Compared to as-grown TNRs, the annealed one has lower electrical resistivity attributed to lower defect concentration as shown by the XPS results. It is the benefit for the electronic transmission, which could lead to a higher efficiency.

4. Conclusions

In summary, the effect of thermal treatment on TNRs generated with the solvothermal method was studied in detail using TiO₂ nanorod arrays as an example. The results show that thermal treatment does not change the crystal structure of TiO₂ but does significantly improve the surface condition of TiO₂ nanorods by converting an amorphous layer into tiny crystallite spheres. Furthermore, absorbed water and residual n-hexane molecules on the surface of the TNRs disappeared. Dye absorption was significantly enhanced due to the surface reconfiguration and the changes in surface chemical bonds. In addition, the annealed TNR sample has less oxygen vacancy-Ti³⁺-related defects than do the as-grown ones, which improves electron transport. Therefore, a power conversion efficiency of 3.21% is achieved from the annealed TNRs, which is an increase of 39% compared to as-grown TNRs. Our findings could be useful for photoelectrical applications of the solvothermal synthesis method.

Acknowledgments

This work was supported by the National Natural Science Foundation of China (nos. 51372083, 51072051, 51102092, 51302081), the Program for New Century Excellent Talents in University (NCET-11-0636), the Fundamental Research Funds for the Central Universities (nos. 12ZX14, 11QG24, 13ZP07, 13QN21, 13MS127), and the Specialized Research Fund for the Doctoral Program of Higher Education in China (no. 20110036120002).

References

[1] B. O'Regan, M. Grätzel, *Nature* 353 (1991) 737–740.

- [2] M.K. Nazeeruddin, P. Pechy, T. Renouard, S.M. Zakeeruddin, R. Humphry-Baker, P. Comte, P. Liska, L. Cevey, E. Costa, V. Shklover, L. Spiccia, G.B. Deacon, C.A. Bignozzi, M. Grätzel, *J. Am. Chem. Soc.* 123 (2001) 1613–1624.
- [3] M. Grätzel, *J. Photochem. Photobiol. C* 4 (2003) 145–153.
- [4] A. Yella, H.W. Lee, H.N. Tsao, C. Yi, A.K. Chandiran, M.K. Nazeeruddin, E.W. Diau, C.Y. Yeh, S.M. Zakeeruddin, M. Grätzel, *Science* 334 (2011) 629–634.
- [5] X.D. Li, Y.Z. Zhang, Z.X. Zhang, J.Y. Zhou, J. Song, B.A. Lu, E.Q. Xie, W. Lan, *J. Power Sources* 196 (2011) 1639–1644.
- [6] B. Liu, E.S. Aydil, *J. Am. Chem. Soc.* 131 (2009) 3985–3990.
- [7] M. Law, L.E. Greene, J.C. Johnson, R. Saykally, P. Yang, *Nat. Mater.* 4 (2005) 455–459.
- [8] S.M. Wang, W.W. Dong, R.H. Tao, Z.H. Deng, J.Z. Shao, L.H. Hu, J. Zhu, X.D. Fang, *J. Power Sources* 235 (2013) 193–201.
- [9] Z.R. Wang, H. Wang, B. Liu, W.Z. Qiu, J. Zhang, S.H. Ran, H.T. Huang, J. Xu, H.W. Han, D. Chen, G.Z. Shen, *ACS Nano* 5 (2011) 8412–8419.
- [10] K. Zhu, N.R. Neale, A.F. Halverson, J.Y. Kim, A.J. Frank, *J. Phys. Chem. C* 114 (2010) 13433–13441.
- [11] L.L. Yang, Q.X. Zhao, M. Willander, J.H. Yang, I. Ivanov, *J. Appl. Phys.* 105 (2009) 053503.
- [12] Q. Zhao, X.Y. Xu, X.F. Song, X.Z. Zhang, D.P. Yu, C.P. Li, L. Guo, *Appl. Phys. Lett.* 88 (2006) 033102.
- [13] K.F. Huo, X.M. Zhang, J.J. Fu, G.X. Qian, Y.C. Xin, B.Q. Zhu, H.W. Ni, P.K. Chu, *J. Nanosci. Nanotechnol.* 9 (2009) 3341–3346.
- [14] N.-G. Park, G. Schlichthörl, J.v.d. Lagemaat, H.M. Cheong, A. Mascarenhas, A.J. Frank, *J. Phys. Chem. B* 103 (1999) 3308–3314.
- [15] Z.J. Zhou, J.Q. Fan, X. Wang, W.H. Zhou, Z.L. Du, S.X. Wu, *ACS Appl. Mater. Interfaces* 3 (2011) 4349–4353.
- [16] J. Zhou, B. Song, G.L. Zhao, W.X. Dong, G.R. Han, *Appl. Phys. A* 107 (2012) 321–331.
- [17] Y.Z. Zhang, L.H. Wu, Y.P. Liu, E.Q. Xie, *J. Phys. D Appl. Phys.* 42 (2009) 085105.
- [18] J. Chung, J. Lee, S. Lim, *Physica B* 405 (2010) 2593–2598.
- [19] F.D. Angelis, S. Fantacci, A. Selloni, M. Grätzel, M.K. Nazeeruddin, *Nano Lett.* 7 (2007) 3189–3195.
- [20] P. Falaras, *Sol. Energy Mater. Sol. Cells* 53 (1998) 163–175.
- [21] K.E. Lee, M.A. Gomez, S. Elouatik, G.P. Demopoulos, *Langmuir* 26 (2010) 9575–9583.
- [22] F. Shao, J. Sun, L. Gao, S. Yang, J. Luo, *J. Math. Chem.* 22 (2012) 6824.
- [23] X.B. Zhang, H.M. Tian, X.Y. Wang, G.G. Xue, Z.P. Tian, J.Y. Zhang, S.K. Yuan, T. Yu, Z.G. Zou, *Mater. Lett.* 100 (2013) 51–53.
- [24] K.J. Wu, K. Shen, W.F. Liu, L.E. Wu, D.L. Wang, *Phys. Stat. Sol. A* 209 (2012) 1369–1375.
- [25] L. Zhao, M.D. Han, J.S. Lian, *Thin Solid Films* 516 (2008) 3394–3398.
- [26] Y.F. Gao, Y. Masuda, K. Koumoto, *Langmuir* 20 (2004) 3188–3194.
- [27] Y. Yu, K.J. Wu, D.L. Wang, *Appl. Phys. Lett.* 99 (2011) 192104.
- [28] J. Lagowski, E.S. Sproles, H.C. Gatos, *J. Appl. Phys.* 48 (1977) 3566.
- [29] Y.Z. Zhang, L.H. Wu, E.Q. Xie, H.G. Duan, W.H. Han, J.G. Zhao, *J. Power Sources* 189 (2009) 1256–1263.
- [30] Y.X. Zhang, G.H. Li, Y.C. Wu, Y.Y. Luo, L.D. Zhang, *J. Phys. Chem. B* 109 (2005) 5478–5481.
- [31] V.A. Nadtochenko, A.G. Rincon, S.E. Stanca, J. Kiwi, *J. Photochem. Photobiol. A* 169 (2005) 131–137.
- [32] M.S. Hamdy, O. Berg, J.C. Jansen, T. Maschmeyer, J.A. Moulijn, G. Mul, *Chemistry* 12 (2005) 620–628.
- [33] T. Bezrodna, G. Puchkovska, V. Shymanovska, J. Baran, H. Ratajczak, *J. Mol. Struct.* 700 (2004) 175–181.
- [34] P. Jackson, G.D. Parfitt, *Trans. Faraday Soc.* 67 (1971) 2469–2483.
- [35] Z.J. Li, B. Hou, Y. Xu, D. Wu, Y.H. Sun, *J. Colloid Interface Sci.* 288 (2005) 149–154.
- [36] S. Karuppuchamy, J.M. Jeong, *Mater. Chem. Phys.* 93 (2005) 251–254.
- [37] J.L. Lan, T.C. Wei, S.P. Peng, C.C. Wan, G.Z. Cao, *J. Phys. Chem. C* 116 (2012) 25727–25733.
- [38] F. Fabregat-Santiago, J. Bisquert, G. Garcia-Belmonte, G. Boschloo, A. Hagfeldt, *Sol. Energy Mater. Sol. Cells* 87 (2005) 117–131.
- [39] K.M. Guo, M.Y. Li, X.L. Fang, X.L. Liu, B. Sebo, Y.D. Zhu, Z.Q. Hu, X.Z. Zhao, *J. Power Sources* 230 (2013) 155–160.
- [40] M. Adachi, M. Sakamoto, J. Jiu, Y. Ogata, S. Isoda, *J. Phys. Chem. B* 110 (2006) 13872–13880.
- [41] B. PerezGarcia, J. ZunigaPerez, V. MunozSanjose, J. Colchero, E. PalaciosLidon, *Nano Lett.* 7 (2007) 1505–1511.